Journal of Applied Nonlinear Dynamics 7(2) (2018) 123-129

Journal of Applied Nonlinear Dynamics

https://lhscientificpublishing.com/Journals/JAND-Default.aspx

On the Localization of Invariant Tori in a Family of Generalized Standard Mappings and its Applications to Scaling in a Chaotic Sea

Diogo Ricardo da Costa[1†], Iberê L. Caldas[2], Denis G. Ladeira[3], Edson D. Leonel[4]

[1] Departamento de Física, UNESP - Univ Estadual Paulista, Av.24A, 1515, 13506-900, Rio Claro, SP - Brazil

[2] Instituto de Física da USP, Rua do Matão, Travessa R, 187 - Cidade Universitária, 05314-970, São Paulo, SP - Brazil

[3] Universidade Federal de São João Del-Rei, Departamento de Física e Matemática. Rodovia MG 443, Km 07, 36420-000, Ouro Branco, MG - Brazil

[4] Abdus Salam International Center for Theoretical Physics, Strada Costiera 11, 34151 Trieste, Italy

Submission Info

Communicated by A.C.J. Luo
Received 14 February 2017
Accepted 25 May 2017
Available online 1 July 2018

Keywords

Chaos
Invariant tori
Generalized standard mappings
Chaotic sea

Abstract

The localization of the last invariant spanning curve – also known as the last invariant tori – in a family of generalized standard mappings is discussed. The position of the curve dictates the size of the chaotic sea hence influencing the scaling properties observed for such region. The mapping is area preserving and is constructed such its dynamical variables are the action, J, and the angle θ. The action is controlled by a parameter ε, controlling the intensity of a generic nonlinear function, which defines a transition from integrable for $\varepsilon = 0$ to non integrable for $\varepsilon \neq 0$. The angle is dependent on a parameter γ. If $\gamma > 0$, the angle has the property that it diverges in the limit of vanishingly action and is added, by a finite function dependent on a free parameter γ, when the action is larger than zero. The case $\gamma = -1$ reproduces the expression of the angle for the traditional standard mapping. The phase space is mixed and shows, for certain ranges of control parameters, a set of periodic islands, chaotic seas and invariant spanning curves. Statistical properties for an ensemble of noninteracting particles starting in the chaotic sea with very low action is considered and we show: (i) the saturation of chaotic orbits grows with ε^{α}; (ii) the regime of growth scales with n^{β}; and (iii) the regime that marks the changeover from the diffusive dynamics to the stationary state scales with ε^{z}. The exponents α and z depend on γ and are independent of the nonlinear function f while β is universal. To illustrate the theory here proposed, we obtain an estimation for the critical parameter K_c for a generalized standard mapping considering three different periodic functions. We also find α, β and z for different nonlinear functions.

†Corresponding author.
Email address: diogocost2@gmail.com

ISSN 2164-6457, eISSN 2164-6473/$-see front materials
DOI:10.5890/JAND.2018.06.002

After the seminal paper from Moser [1] discussing the conditions for the existence of invariant curves for area preserving mappings of an annulus, the subject and interest for the topic increased significantly. The invariant curve has the property of separate different portions of the phase space. Therefore it blocks the passage of particles through it. Because of its crucial importance in transport properties and on the scaling in chaotic seas, among other applications, many different recent investigations were carried out. As for example, the Slater criteria [2], which precedes to Moser results, was used to estimate the breakup of invariant curves in dynamical systems [3] and to prove the existence of non-twist phenomenon in reversible non Hamiltonian systems [4]. Moreover, elementary proofs of the existence and of some properties of non autonomous analogues of rotational tori are discussed in [5] while the construction of a tori in the phase space and the inverse problem of Poincaré was made in [6]. Analytical results were made also to understand the topic, particularly the works of Wang [7], who has made investigation of the destruction of invariant circles for Gevrey area preserving twist map, Gentile [8] studying invariant curves for exact symplectic twist maps of the cylinder with Bryuno rotation numbers and Kaloshin and Zhang [9] who gave a proof of a strong form of Arnold diffusion for smooth convex Hamiltonian systems.

In this letter we describe how to construct a family of generic mapping by using a Hamiltonian formalism similar as the one used in [10]. We consider a function describing the angle with the following properties: (i) is a continuous function; (ii) is controlled by a parameter γ. For $\gamma = -1$ the expression of the angle for the standard map [11] is recovered and; (iii) for $\gamma > 0$ the angle diverges in the limit of vanishingly action. The variable action is dependent on a parameter ε controlling the intensity of a generic nonlinear function f which is smooth, continuous, infinitely many differentiable and periodic. Our main goal is to understand, obtain and describe how the position of the lowest action invariant spanning curve influences the scaling features of the chaotic sea in the low energy regime particularly focusing on the description of the observable $J_{rms} = \sqrt{\overline{J^2}}$ at the short, intermediate and long time dynamics. As we will see, three control parameters are important in order to understand the behaviour of J_{rms}, named α, β and z. We will show how to find them for any nonlinear function chosen. In order to to this, it is necessary to obtain an estimation for the critical parameter K_c for a generalized standard mapping.

To start we consider the following Hamiltonian $H(J_1, J_2, \theta_1, \theta_2) = H_0(J_0, J_1) + \varepsilon H_1(J_0, J_1, \theta_0, \theta_1)$, where the variables J_l and θ_l with $l = 1, 2$ correspond respectively to the action and angle [10]. The term H_0 corresponds to the integrable part of the Hamiltonian while H_1 is a non integrable contribution. The parameter ε controls a transition from integrability, from $\varepsilon = 0$, to non integrability with $\varepsilon \neq 0$. Because the Hamiltonian is time independent, one of the four variables can be eliminated, say J_2, and only three are left. A Poincaré surface of section defined by the plane $J_1 \times \theta_1$ at θ_2 constant (mod 2π) is considered. As a result, the perturbed twist mapping is given by $J_{n+1} = J_n - \varepsilon f(J_{n+1}, \theta_n)$ and $\theta_{n+1} = \theta_n + \kappa(J_{n+1}) + \varepsilon g(J_{n+1}, \theta_n)$, where f and g are periodic functions in θ. The function $F_2 = J_{n+1}\theta_n + A(J_{n+1}) + \varepsilon \tilde{f}(J_{n+1}, \theta_n)$ generates the previous mapping, with $\kappa = dA/dJ_{n+1}$, $f = \partial \tilde{f}/\partial \theta_n$ and $g = \partial \tilde{f}/\partial J_{n+1}$. For area preservation, the expression $\frac{\partial g}{\partial \theta_n} - \frac{\partial f}{\partial J_{n+1}} = 0$ needs to be satisfied. For many mappings $g(J_{n+1}, \theta_n) = 0$ ($\tilde{f}$ is independent of J_{n+1}), therefore the following mapping is obtained [10]

$$T : \begin{cases} J_{n+1} = J_n - \varepsilon f(\theta_n), \\ \theta_{n+1} = \theta_n + \kappa(J_{n+1}) \quad \mathrm{mod}(2\pi). \end{cases} \tag{1}$$

When $g = 0$ and $\tilde{f}(\theta_n) = \cos(\theta_n)$, many applications can be found in the literature [10]. To illustrate few of them, the standard mapping is reproduced considering $\kappa(J_{n+1}) = J_{n+1}$ [11]. For $\kappa = 2/J_{n+1}$ the Fermi-Ulam model is reproduced [12, 13]. $\kappa = \zeta J_{n+1}$, where ζ is a constant, describes the bouncer model [14]. For $\kappa(J_{n+1}) = J_{n+1} + \zeta J_{n+1}^2$, the logistic twist mapping is obtained [15]. An application merging properties of the Fermi-Ulam [12] and bouncer [14] leading to a the hybrid Fermi-Ulam bouncer model can be seen in [16].

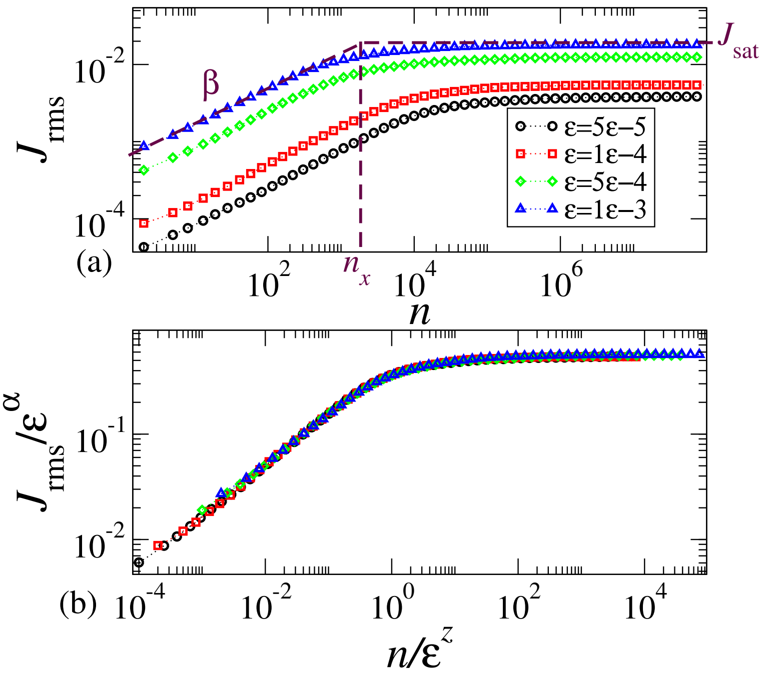

Fig. 1 Plot of: (a) J_{rms} *vs.* n for different values of ε and considering $\tilde{f} = \cos(\theta)$ in mapping (1). (b) After a properly rescale in the axis, all curves overlapped onto each other in a single and hence universal curve. The parameters used were $\gamma = 1$ and $M = 1000$ different initial conditions chosen as $J_0 = 10^{-3}\varepsilon$ and $\theta_0 \in [0, 2\pi)$.

As one of the properties of f, we assume it is a smooth and periodic function such that $f(\theta) = f(\theta + 2\pi)$. For $\kappa(J_{n+1}) = J_{n+1}$, and choosing $\tilde{f} = \cos(\theta)$ the standard map is recovered [10]. For $\varepsilon < K_c \cong 0.9716\ldots$, the standard map has invariant spanning curves which prevent the chaos to diffusing unlimitedly. For $\varepsilon > K_c$ a chaotic sea can widespread unlimitedly from $\pm\infty$ in action axis. In our approach we consider that $\kappa(J_{n+1}) = -|J_{n+1}|^{-\gamma}$ in the mapping (1), where γ is a control parameter. $\gamma = -1$ yields the standard mapping [11] while $\gamma = 1$ gives the Fermi-Ulam [12, 13]. For $\gamma = 3/2$ the Keppler map is recovered [17]. The phase space of the mapping is mixed and contains periodic islands, invariant spanning curves and chaotic seas. We are interested in the scaling properties of the chaotic sea considering $\gamma > 0$. Then, we describe the dynamics under three regimes: (i) short time; (ii) long time and; (iii) intermediate time.

We begin with case (i). For short time and starting the dynamics using an ensemble of initial conditions in the low action regime along the chaotic sea, the ensemble of particle evolves using mapping (1). The first equation of mapping (1) is written as $J_{n+1}^2 = J_n^2 - 2J_n\varepsilon f(\theta_n) + \varepsilon^2[f(\theta_n)]^2$, where $f(\theta_n)$ attends to the conditions above. Moreover, it has a well defined average so that averaging the equation over an ensemble of $\theta \in [0, 2\pi]$, we obtain $\overline{J_{n+1}^2} = \overline{J_n^2} + \frac{\varepsilon^2}{2\pi}c(f)$, where $c(f)$ is a constant that depends on the f chosen and is written as $c(f) = \int_0^{2\pi}[f(\theta_n)]^2 d\theta_n$. An important observation that needs to be taken into account is that $\int_0^{2\pi}[f(\theta_n)]d\theta_n = 0$ for any function f. For sufficiently small ε, we use the following approximation $\overline{J_{n+1}^2} - \overline{J_n^2} = \frac{\overline{J_{n+1}^2} - \overline{J_n^2}}{(n+1)-n} \cong \frac{d\overline{J^2}}{dn} = \frac{\varepsilon^2}{2\pi}c(f)$. After a direct integration we have $J_{rms}(n) = \sqrt{J_0^2 + \frac{\varepsilon^2}{2\pi}c(f)n}$.

Figure 1(a) shows a plot of J_{rms} *vs.* n. We see that for short n, J_{rms} can be described as $J_{rms} \propto n^{\beta}$. A power law fit for short n gives $\beta \approx 0.5$. For large enough n the regime of growth is changed to a saturation. In our simulations J_{rms} was obtained as $J_{rms} = \sqrt{\overline{J^2}} = \sqrt{\frac{1}{M}\sum_{i=1}^{M}[\frac{1}{n}\sum_{j=1}^{n}J_{i,j}^2]}$, where M is the number of different initial conditions. Analyzing J_{sat}, where the subindex *sat* indicates saturation, as

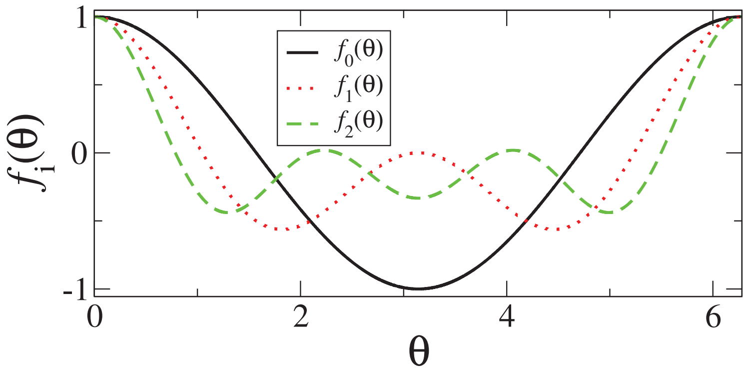

Fig. 2 Plot of the functions $f_i(\theta)$ against θ for $\theta \in (0, 2\pi]$ with $i = 0, 1, 2$.

function of the parameter ε, a law $J_{sat} \propto \varepsilon^{\alpha}$ is obtained. Therefore, the saturation of J has a link to the position of the first invariant spanning curve, indeed a fraction of it, which depends on the parameter γ and not on the function $\tilde{f}$. Our simulations for $\gamma = 1$ lead to an exponent $\alpha \cong 0.5$.

Let us now discuss the saturation given by case (ii), i.e., large enough time. The exponent α indirectly controls the position of the lowest invariant spanning curve denoted as J^*. Near the spanning curve, the dynamics of the mapping can be made locally via a connection with the generalized standard mapping. We assume then $J_{n+1} = J^* + \Delta J_{n+1}$ where ΔJ_{n+1} is a small perturbation of the curve. We stress $J^* > 0$ and $\varepsilon > 0$ so that the absolute value of $|J_{n+1}|$ is simply written as J_{n+1}. Considering the second equation of Map (1) and Taylor expanding under the limit $\Delta J_{n+1}/J^* \to 0$ we end up with $\theta_{n+1} = \theta_n + I_{n+1}$, where $I_{n+1} = \gamma \Delta J_{n+1}(J^*)^{-(1+\gamma)} - (J^*)^{-\gamma}$.

Rewriting the first equation of mapping (1), multiplying both sides by $\gamma J^{*-(1+\gamma)}$, adding $-J^{*-(1+\gamma)}$ in both sides of the equation and rearranging the terms, the following expression is obtained $I_{n+1} = I_n - \gamma \varepsilon J^{*1+\gamma} f(\theta_n)$. These changes lead to the following map

$$\begin{cases} I_{n+1} = I_n - \dfrac{\gamma\varepsilon}{J^{*(1+\gamma)}} f(\theta_n), \\ \theta_{n+1} = (\theta_n + I_{n+1}) \mod 2\pi. \end{cases} \tag{2}$$

This mapping is structurally the same of the generalized standard mapping and the term $\gamma\varepsilon/J^{*(1+\gamma)}$ corresponds to a local parameter $K_c(f)$ in the generalized standard mapping which marks the transition from local to global chaos $K_c = \gamma \varepsilon J^{*-(1+\gamma)}$.

For each given function f a different K_c is obtained. Therefore, the position of the first invariant spanning curve is $J^* = [\frac{\gamma\varepsilon}{K_c(f)}]^{\frac{1}{(1+\gamma)}}$. In a more simplified way, it is written as $J^* \propto \varepsilon^{\frac{1}{1+\gamma}}$. This expression allows an immediate comparison with the exponent α, so that $\alpha = (1+\gamma)^{-1}$, resulting in $J^* \propto \varepsilon^{\alpha}$, as mentioned in [18].

When the regime of growth meets with the saturation, case (iii) applies. Matching the equation of growth with the one marking the saturation we end up with $\frac{n_x = \frac{2\pi}{c(f)}[\gamma}{K_c(f)]^{\frac{2}{(1+\gamma)}} \varepsilon^{\frac{-2\gamma}{1+\gamma}}}$. As it is known in the literature [18], $n_x \propto \varepsilon^z$, hence $z = \frac{-2\gamma}{1+\gamma}$ which also proves that z is independent on the function f.

After obtaining the values of α and z, all curves in Fig. 1(a) overlap onto each other in a single and universal curve with the following scaling transformations $n \to n/\varepsilon^z$ and $J_{rms} \to J_{rms}/\varepsilon^{\alpha}$ as shown in Fig. 1(b).

Let us now discuss the localization of the invariant spanning curve for a more general function f, hence considering a generalized standard mapping with $\gamma = -1$. We consider the following cases $f(\theta) = f_i(\theta)$, with $i = 0, 1, 2$, hence $f_0(\theta) = \cos(\theta)$, $f_1(\theta) = \frac{1}{2}[\cos(\theta) + \cos(2\theta)]$ or $f_2(\theta) =$

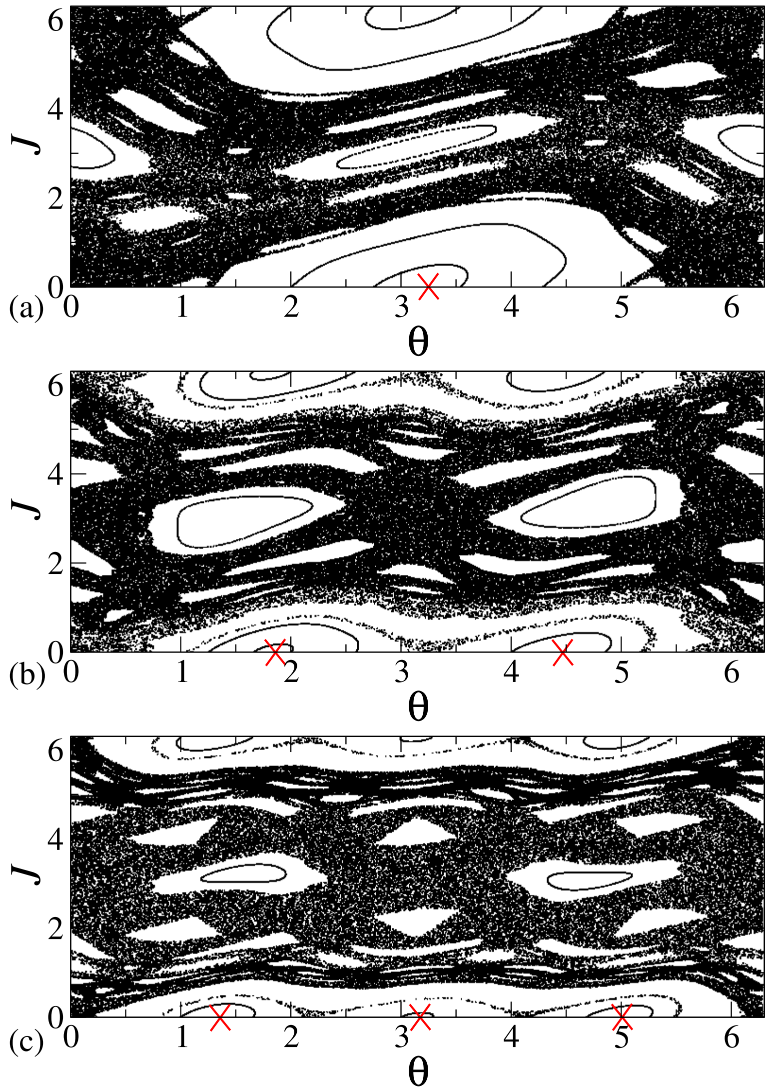

Fig. 3 Plot of the phase space for: (a) $f_0(\theta)$ and $\varepsilon = 1.2$; (b) $f_1(\theta)$ and $\varepsilon = 0.5$; (c) $f_2(\theta)$ and $\varepsilon = 0.24$. The parameter γ was fixed at $\gamma = 1$. The mixed structure of the phase space is evident in both figures.

$\frac{1}{3}[\cos(\theta)+\cos(2\theta)+\cos(3\theta)]$. A pure cosine function ($i = 0$) is our reference, as shown in Fig. 2. Figure 3(a) shows a phase space for $f = f_0$ and considering $\varepsilon = 1.2$. The phase space is clearly mixed-type, containing periodic islands and a large chaotic sea. This parameter produces a global chaos because unlimited diffusion in the action may occurs, while only limited diffusion is observed for $\varepsilon < K_c$. We then search for values of K_c in the different functions f_i chosen.

A phase space for $f = f_1$ and $\varepsilon = 0.5$ is shown in Fig. 3(b), and the red crosses mark a period 2 fixed point. The period of the lowest periodic fixed point depends on which i is used. For example, if $f = f_0$ the period is one (see Fig. 3(a)), but for $f = f_2$ and $\varepsilon = 0.24$ the period is three (see the red crosses in the Fig. 3(c)).

We used the following procedure to estimate numerically K_c for the different function f_i. The method consists of iterate the initial conditions up to $n_{\max} = 10^{11}$ times for different values of the parameter ε. The algorithm stores the minimum value of J of the trajectory associated to the initial condition $(\theta_0, J_0) = (10^{-6}, 10^{-6})$ and, similarly, the maximum value of J of the orbit associated to $(\theta_0, J_0) = (10^{-6}, 2\pi - 10^{-6})$. If the minimum and maximum reach the value $J = \pi$, then we conclude spanning

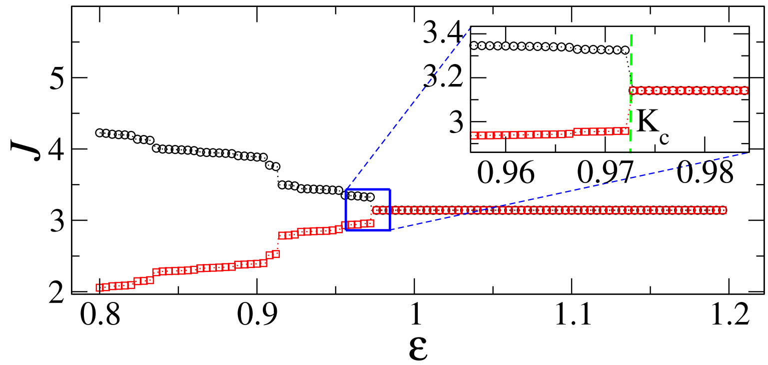

Fig. 4 Plot of minimum value of J found for an orbit starting from $J_0 = 2\pi - 10^{-6}$ and $\theta_0 = 10^{-6}$ until it reaches $J = \pi$. The red squares show the maximum value of J for an orbit starting from $J_0 = 10^{-6}$ and $\theta_0 = 10^{-6}$. The orbits were iterated up to 10^{11} times and the point where these two orbits touch $J = \pi$ is a good estimation for K_c.

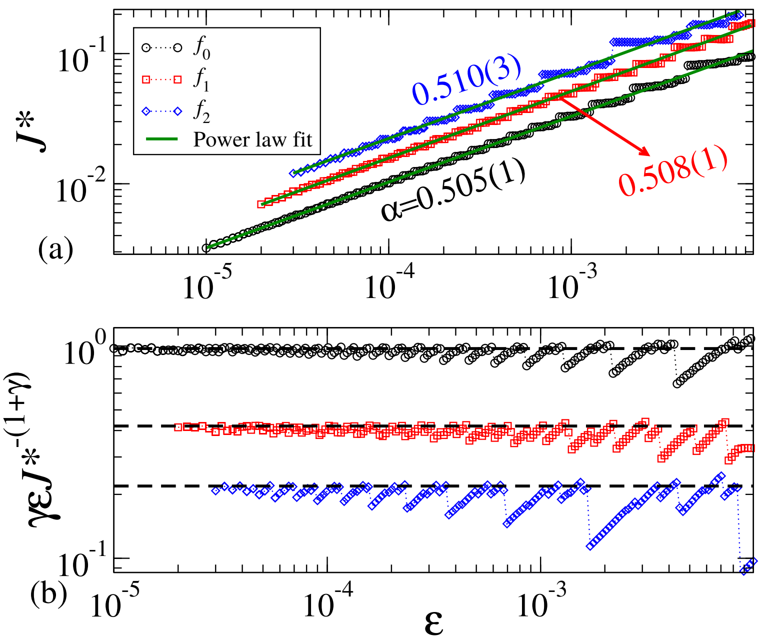

Fig. 5 Plot of: (a) Approximated position for the minimum of the lowest invariant spanning curve (J^*) as function of the control parameter ε. The orbits were iterated up to 10^{11}, and we have considered $J_0 = \theta_0 = 10^{-6}$ and $\gamma = 1$. (b) Rescale in the vertical axis of item (a) $J^* \rightarrow \gamma\varepsilon J^{*-(1+\gamma)}$, where the dashed lines are the values of $K_c(f_i)$ found numerically for the generalized standard mapping.

curves do not exist in phase space. Therefore $\varepsilon \geq K_c$ and the iteration process of the corresponding trajectory is interrupted. Otherwise, both trajectories are iterated up to $n_{\max}$. When parameter ε is chosen such that a crossing from $J = \pi$ happens, another ε must be taken (500 different values of ε were selected in our simulations). In Fig. 4 we present the results for orbits iterated up to $n_{\max}$ times for $f = f_0$. The orbits touch $J = \pi$ simultaneously at $\varepsilon \cong 0.9728$. This value is approximately the same found using Greene's residue criterion [19], which is equal to $K_c = 0.9716\ldots$. The same procedure was used for the functions f_1 and f_2 leading to the values $K_c = 0.42\ldots$ and $K_c = 0.219\ldots$, respectively.

Now we estimate the position of the lowest action invariant spanning curve. For this, we divide $\theta \in (0, 2\pi]$ in a stripe of 10^3 equally spaced cells. For each cell, the highest value of J in the chaotic sea is collected after a long run of $n_{\max}$ iterations of the mapping. With this, an inferior limit for the invariant spanning curve is obtained numerically. Figure 5(a) shows J^* as a function of ε for the initial conditions $J_0 = \theta_0 = 10^{-6}$. The curves are described by a power law of ε with slope $\alpha \cong 1/2$ (the values found were 0.505(1), 0.508(1) and 0.510(3) respectively for f_0, f_1 and f_2. Other values of γ where tested too and result is in good agreement with the theory. Figure 5(b) shows the rescaled axis $J^* \rightarrow \gamma\varepsilon J^{*-(1+\gamma)}$ as a function of ε for the different functions f_i considered. The dashed lines are the critical values K_c found for the generalized standard mapping considering each function f_i. As seen the numerical results are in agreement with the analytical ones (dashed lines). The larger ε the worse is the approximation for K_c.

As a short summary, we obtained the localization of the last invariant spanning curve in a family of generalized standard mappings. An estimation for the critical parameter K_c considering three different periodic functions was found. Theses values were used to compare with the result obtained from theoretical prediction. We also obtain the exponents α, β and z describing the curves of J_{rms} for different values of f_i. We demonstrated that the critical exponents α and z depend on γ and are independent of the nonlinear function f while β is universal.

Acknowledgments

DRC acknowledges Brazilian agencies PNPD/Capes and FAPESP (2013/22764-2). EDL thanks to CNPq (303707/2015-1) and FAPESP (2012/23688-5), Brazilian agencies. This research was supported by resources supplied by the Center for Scientific Computing (NCC/GridUNESP) of the São Paulo State University (UNESP).

References

[1] Moser, J.K. (1962), *Nachr. Akad. Wiss. Göttingen Math.-Phys. Kl II*, **1962**, 1.
[2] Slater, N.B. (1950), *Mathematical Proceedings of the Cambridge Philosophical Society*, **46**, 525.
[3] Abud, C.V., Caldas, I.L., (2015), *Physica D*, **308**, 34.
[4] Altmann, E.G., Cristadoro, G. and Pazó, D. (2006), *Phys. Rev. E*, **73**, 056201.
[5] Canadell, M. and de la Llave, R. (2015), *Physica D*, **310**, 104.
[6] Laakso, T., Mikko, K. (2016), *Physica D*, **315**, 72.
[7] Wang, L. and Dyn. J. (2015), *Diff. Equat.*, **27**, 283.
[8] Gentili, G. (2015), *Nonlinearity*, **28**, 2555.
[9] Kaloshin, V. and Zhang, K. (2015), *Nonlinearity*, **28**, 2699.
[10] Lichtenberg, A.J. and Lieberman, M.A. (1992), *Regular and Chaotic Dynamics, Appl. Math. Sci.*, **38**, Springer, New York.
[11] Chirikov, B.V. (1979), *Phys. Rep.*, **52**, 263.
[12] Lieberman, M.A. and Lichtenberg, A.J. (1971), *Phys. Rev. A*, **5**, 1852.
[13] Karlis, A.K., et. al (2006), *Phys. Rev. Lett.*, **97**, 194102.
[14] Pustylnikov, L.D. (1978), *Trans. Mosc. Math. Soc.*, **2**, 1.
[15] Howard, J.E. and Humpherys, J. (1995), *Physica D*, **80**, 256.
[16] Leonel, E.D. and McClintock, P.V.E. (2005), *J. Phys. A*, **38**, 823.
[17] Petrosky, T. Y. (1986), *Phys. Lett. A*, **117**, 328.
[18] Leonel, E.D., de Oliveira, J.A., and Saif, F. (2011), *Phys. A: Math. Theor.*, **44**, 302001.
[19] MacKay, R.S. (1992), *Nonlinearity*, **5**, 161.